Journal of the Brazilian Society of Mechanical Sciences and Engineering (2020) 42:372
https://doi.org/10.1007/s40430-020-02456-6

TECHNICAL PAPER

Effect of thickness and energy on electromagnetic compression of AA6061 tube

Amitabh Shrivastava[1] · Amit Telang[1] · A. K. Jha[2] · Meraj Ahmed[2]

Received: 17 April 2019 / Accepted: 9 June 2020 / Published online: 17 June 2020

Abstract
Electromagnetic forming (EMF) has many applications in the automobile, structural, and other related areas due to its advantages such as reduced springback, wrinkling, and enhanced formability of deformed parts. Deformation of the workpiece depends on various process parameters such as applied energy level; system parameters such as inductance, capacitance, and resistance; and workpiece geometry such as thickness, and shape. These parameters control the current pulse, magnetic field, and Lorentz force. In the present study, effects of workpiece thickness, applied energy level, and process parameters on the deformation behavior of an AA6061 Al tube were studied. An attempt was also made to correlate discharge energy and process parameters with tube deformation. Finite-element (FE) analysis was performed to validate the experimental results. Various parameters such as the Lorentz force, magnetic field, and current density across the workpiece (tube), which cannot be measured experimentally, were numerically computed and correlated with the resulting nature of tube deformation. Aluminum alloy (AA) 6061 tubes with wall thicknesses of 1, 1.7, and 2.4 mm were deformed using a 4-turn bitter copper coil connected to a 40 kJ capacitor bank. In the present case, the intermediate wall thickness of the workpiece showed a higher efficiency for deformation. Moreover, reasonably good agreement was observed between the experimental and FE-simulated results.

Keywords Electromagnetic forming · High-velocity forming · FE simulation · Aluminum alloy 6061

1 Introduction

High-velocity forming of tubes and sheets has gained popularity among researchers and industrial sectors such as automobiles and aerospace due to several advantages. Several forming operations such as bulging, flaring, forming, compression, and joining are involved in tube processing that leads to the conversion of tubes into useful products. All these operations are possible through a high-velocity forming technique called electromagnetic forming (EMF) or electromagnetic compression (EMC). EMF is a high-energy and high strain rate forming process in which the achieved degree of deformation is more than that achieved through conventional forming methods. Conventional forming processes for the shaping of metallic sheets and tubes result in problems such as springback, wrinkling, non-uniform strain distribution, and poor formability. These limitations can be effectively minimized or alleviated by employing EMF, thus achieving the forming of intricate shapes and complex geometries. Furthermore, the long processing procedure involved during conventional forming can effectively be replaced with the more efficient high-velocity forming technique. During the joining process of EMF, the welded or joined interface becomes free from any impurity and heat-affected zone (HAZ), because the material does not melt or fuse therein. Reduced processing time is another advantage of this process wherein operation is completed in a few microseconds (μs). An EMF system consists of components such as a capacitor bank, coil or actuator, field shaper, and charging and discharging system. The EMF circuit consists of elements that form an inductance–capacitance–resistance

Technical Editor: Adriano Fagali de Souza.

✉ Amitabh Shrivastava
amitabh751@gmail.com

[1] Department of Mechanical Engineering, Maulana Azad National Institute of Technology (MANIT), Bhopal 462003, India

[2] Smart and Functional Materials Division, Advanced Materials and Processes Research Institute (AMPRI), Bhopal 462026, India

(L–C–R) circuit. The current pulse flowing through the circuit is greatly influenced by the coil design, capacitor banks, and discharge energy. Thus, it is necessary to analyze the various aspects of design and development when an EMF process is applied for product development involving joining or assembling. Haiping et al. [1] established a relation between the magnetic pressure and length of the coil, with good agreement between numerical and experimental results. The work proved to be crucial for sheet metal and axisymmetric tube forming. An initial work related to the process simulation, which was reported by Bartels et al. [2], involved the development of two coupling models and a comparison of different simulation algorithms for tube compression. Shabanpour et al. [3] studied tube EMC, and the effect of discharge voltage, workpiece thickness, and clearance between die and workpiece on the bead formation depth, wherein the Johnson–Cook damage criteria were developed for a high strain rate process. Haratmeh et al. [4] studied the application of EMF for tube compression. The tube compression experiments were performed and verified numerically in this study. Savadkoohian et al. [5] analyzed the effect of various parameters on wrinkling during tube compression. Even in this work, numerical results were verified with experimental ones. Demir et al. [6] studied tube wrinkling during EMC using the finite-element method (FEM) simulations. Gharghabi et al. [8] attempted the optimization of various process parameters while observing their effect on the nature of deformation. Zhong et al. [9] analyzed the tube bulging process using ANSYS/Emag software. They performed experiments to study displacement, discharge energy, and magnetic pressure. Park et al. [10] reported a parametric study involving numerical simulation for a DP780 steel workpiece with an aluminum driver sheet using a flat spiral coil. Cui et al. [11] studied the multiphysics field simulation of the electromagnetic tube bulging process wherein an FE model was developed and experimentally verified. Haiping et al. [12] analyzed the effect of frequency using the FEM through the sequential coupling method. Ahmed et al. [13] reported the effect of a flat coil on the spatial distribution of coil turns and the distribution of magnetic force, magnetic field, and current density during sheet metal forming. Parameters such as geometry and coil design were emphasized while comparing the response of uniform and non-uniform coils in the study. Moreover, the inductance of both the coils was computed using the FEM, and the same was varied by the inductance calculated using an empirical formula. Vivek et al. [14] studied the extent of deformation during tube compression at different energy levels. Shang et al. [15] performed FE modeling of the tube expansion process and proposed several models. Cao et al. [16] proposed the reduction of coil temperature by employing a crowbar circuit and joule heating without affecting the process and reported the results of numerical and experimental investigations on the effect of the crowbar circuit. By employing the FEM, Rajak et al. [17] analyzed the crimping of an aluminum terminal with a cable using an electromagnetic joining process. Li et al. [18] reported the distribution of magnetic pressure on different tube lengths during the bulging process by developing and experimentally verifying an FE model. Psyk et al. [20] explained several benefits of EMF such as creating typical geometries that are not possible by the conventional methods of deformation. Doley et al. [21] microscopically examined microhardness, HAZ, and the nature of the joint introduced through EMF. Zhang et al. [22] investigated the joining of multi-layer sheets with 2.5–3% interference-fit by employing electromagnetic riveting. Using a copper field shaper, Wang et al. [23] studied aluminum alloy (AA) 6063 tube compression by varying the slope angle and optimizing it. The slot gap in the field shaper has been reported to be responsible for non-uniform deformation.

The above-mentioned review demonstrates the scarcity of studies about the effect of thickness and energy levels of the capacitor bank on tube deformation. Accordingly, an analysis of the relation of deformation behavior of the tube workpiece with the applied energy level and tube thickness was performed in the present work. AA6061 tubes of different wall thicknesses were experimentally deformed using different energy levels and varying number of capacitor banks, thus changing the capacitance of the system. The extent and nature of the deformation were correlated with the tube thickness and energy level. FE simulation was performed to study the deformation behavior of the tube as a function of various parameters such as Lorentz force, magnetic field, current density, and velocity. These parameters were correlated with the tube wall thickness and applied energy level. The experimental results were verified with the FE simulation ones.

2 Experimental

2.1 Material and geometry

2.1.1 Tube material and geometry

In the present study, AA6061 was used as the tube (workpiece) material. The alloy was T6 heat-treated involving solutionizing and artificial aging. It possesses good weldability, and is widely used in applications such as structural components, automobile body, and aerospace parts. The chemical composition of the alloy determined using an optical emission spectrometer (Table 1). In this work, tubes of 56 mm outer diameter and wall thicknesses of 1, 1.7, and 2.4 mm were used. The physical and mechanical properties of AA6061-T6 are presented in Table 2 [7], and flow

Table 1 Chemical compositions of Al alloy (tube)

Alloy	Elements wt%					
	Cu	Fe	Si	Mg	Mn	Al
AA6061	0.18	0.57	0.73	0.51	0.092	Remaining

Table 2 Physical and mechanical properties of Al alloy AA6061-T6 [7]

Alloy	Properties	Value
AA6061-T6	Poisson's ratio	0.33
	Density	2700 (kg/m^3)
	Young's modulus	69 (GPa)

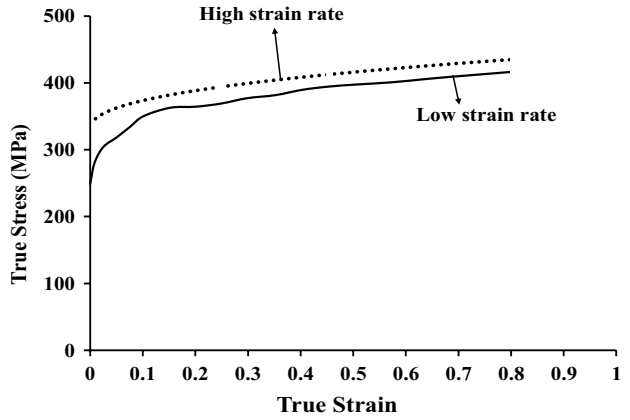

Fig. 1 The true stress versus true strain plots for the experimental workpiece material (AA6061 Al alloy in T6 heat-treated condition) at quasi low and high strain rate [7, 15]

stress of the material at quasi-static and high strain rates is illustrated in Fig. 1.

2.1.2 Coil material and geometry

The coil was made of oxygen-free high thermal conductivity copper that has high electrical conductivity. The outer and inner diameters of the coil were 200 and 57 mm, respectively, with the coil width being 15.6 mm (Fig. 2). The material properties of the coil are presented in Table 3 [19]. The effective number of bitter coil turns was 3, with the cross section of turns being 3 mm × 71.5 mm.

2.2 Experimental setup

The experiments were conducted on a 40 kJ EMF machine. This system consisted of 4 capacitor banks having a total capacitance of 224 μF that can operate at a frequency of 10–15 kHz. In the present study, only 2 capacitor banks were used. Capacitor bank combinations, capacitance, and corresponding energy levels used for the experiments are presented in Table 4. The tubes were deformed at different energy levels obtained by suitably varying the input voltage. The charged capacitor was discharged through the compression coil. The workpiece tube was placed inside the coil that was connected to the capacitor bank through a spark gap switch. A schematic diagram of the experimental setup is shown in Fig. 3. The machine setup consisted of a programmable logic controller-based human–machine interface that enables the selection of the desired voltage for experiments.

The experiments were performed on an AA6061-T6 tube with different wall thicknesses (Table 5) at a constant gap of 0.5 mm between the coil and tube. A highly electrical insulation Kapton tape was used on the outer side of the workpiece (tube) or inner side of the 4-turn compression coil for the prevention of high current hazard. The thicknesses of the tubes considered for the study were 1, 1.7, and 2.4 mm, and they were correspondingly designated as w_1, w_2, and w_3. An experimental matrix showing various parameters is presented in Tables 5 and 6. It exhibits a combination of parameters such as tube wall thickness, the gap between the coil and tube, and the energy or capacitor bank. The discharging current pulse was measured by the Rogowski coil and oscilloscope. The Rogowski coil had a sensitivity of 0.01 mV/A. A digital Vernier caliper with the least count of 0.01 mm was used for measuring the dimensions of the tube before and after deformation.

2.3 FE simulation

The numerical simulation of the process was performed using the LS-DYNA software to validate it with experimental data. Computer-aided design models of the coil and workpiece were developed as per the dimensions taken during the experiments. Corresponding coil and workpiece models were developed as discussed in Sect. 2. The coil and workpiece were meshed with hexahedral three-dimensional elements. The FEM models illustrating the mesh are presented in Fig. 4. The convergence analysis of the model was performed by generating the mesh of different element sizes. Details of elements used for the study are listed in Table 7. The input material properties of the aluminum tube used for the modeling purpose are shown in Fig. 1. Current density, magnetic force, Lorentz force, resultant velocity, and displacement were obtained from the simulation study.

Apart from the general cards used to setup the LS-DYNA program, certain specific cards were also used to

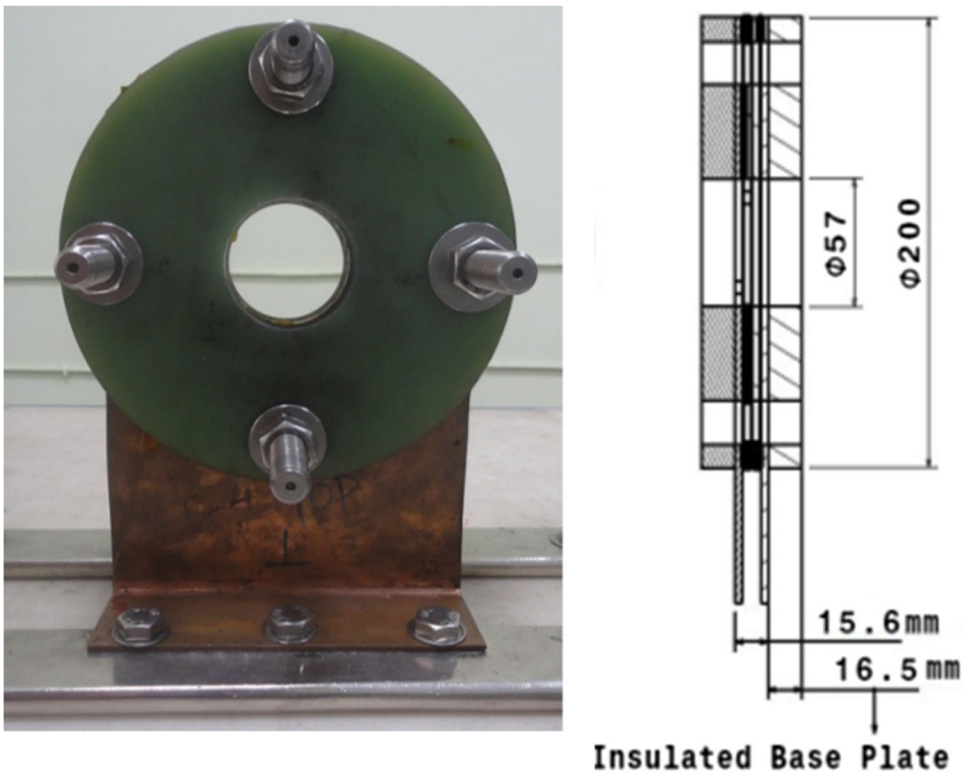

Fig. 2 The photograph of experimental compression coil with section view

Table 3 Mechanical properties of OFHC copper coil [19]

Material	Properties	
OFHC copper	Poisson's ratio	0.34
	Density	8960 (kg/m^3)
	Young's modulus	124 (GPa)

Table 4 Capacitor bank combinations and corresponding energy levels attained during the experiments

Capacitor bank combinations	Capacitance (μF)	Energy (kJ)
Single bank	56	2.8
		4.0
		5.5
		7.2
Double bank	112	8.0

design the material properties and boundary conditions. The material properties of AA6061 were assigned using the MAT_PIECEWISE_LINEAR_PLASTICITY_024 card, and material properties of the copper coil were assigned using the *MAT_ELASTIC_001 card. Current pulse obtained during the experiments using the Rogowski coil was defined using the card *DEFINE_CURVE and assigned to the model through set segments. The current pulse obtained and used in the model is depicted in Fig. 5. The tube was fixed by all degrees of freedom at the upper and lower ends using *BOUNDARY_SPC_SET. The simulation of the tube was performed for varying process parameters. The input energy/voltage was varied at an interval of 2 kV for the entire range of 10–16 kV.

3 Results and discussion

The results of numerical simulation of tube deformation were validated through experimental results. A single capacitor bank was used for 1, 1.7, and 2.4 mm-thick tubes at energy levels of 2.8, 4.0, 5.5, and 7.2 kJ and a gap of 0.5 mm between the coil and tube. Similarly, a double capacitor bank was used for 1.0, 1.7, and 2.4 mm-thick tubes at an energy level of 8.0 kJ. A constant gap of 0.5 mm was maintained between the coil and tube for all the cases. The peak current in the coil increased with the increasing energy level.

Table 8 presents the details of parameters, and experiments and numerical simulation results in terms of the change in tube diameter (OD). For tube w_1, when 12 kV/4.0 kJ was applied using a single capacitor bank, the OD changed from 56 to 51.23 mm. Under similar conditions, the numerically computed OD after deformation was 51.82 mm. Thus, there was an error of 1.14% in this case. Thus, Table 8 shows that the percentage difference in the diameter change between the experimental and numerically simulated results is within acceptable limits, with a

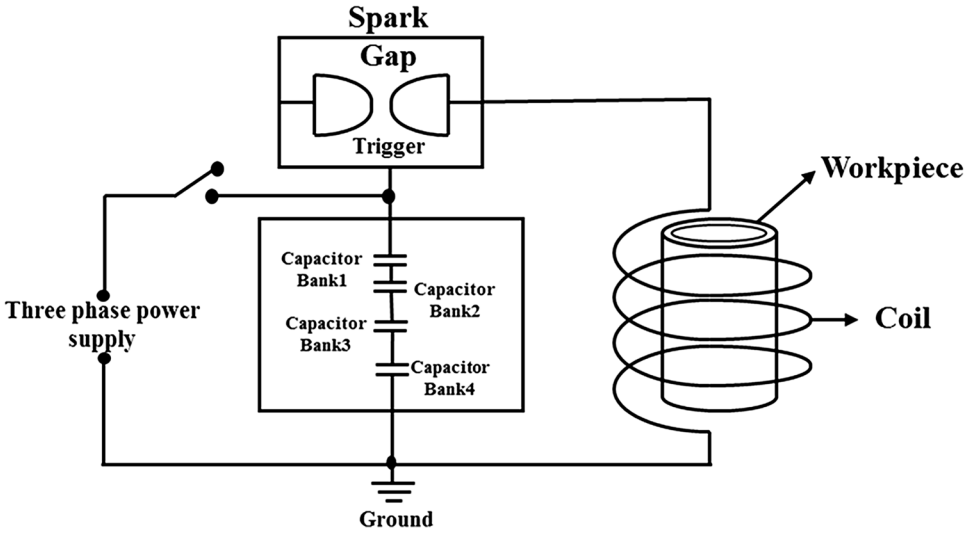

Fig. 3 The schematic representation of the electromagnetic forming test setup

Table 5 Dimensions of the workpiece (tube) and the gap between the workpiece and the coil

Workpiece code	OD (mm)	ID (mm)	Thickness (mm)	Length (mm)	Gap (mm)
w_1	56	54	1	52	0.5
w_2	56	52.6	1.7	52	0.5
w_3	56	51.2	2.4	52	0.5

maximum error in the range of 3–4%. The results of the tube deformed using a double capacitor bank were also within an acceptable range of less than 8% difference when the experimental diameter was compared to the numerical one.

The simulation analysis was performed to observe the effects of parameters such as the energy level, number of capacitor banks, and tube thickness on the nature of deformation. All the parameters that control the deformation behavior of the tube such as current density, magnetic field,

Table 6 Experimental matrix

Single bank (56 μF)						Double bank (112 μF)		
Workpiece	Gap (mm)	Energy (kJ)/voltage (kV)				Workpiece	Gap (mm)	Energy (kJ)/voltage (kV)
w_1	0.5	2.8/10	4.0/12	5.5/14	7.2/16	w_1	0.5	8.0/12
w_2						w_2		
w_3						w_3		

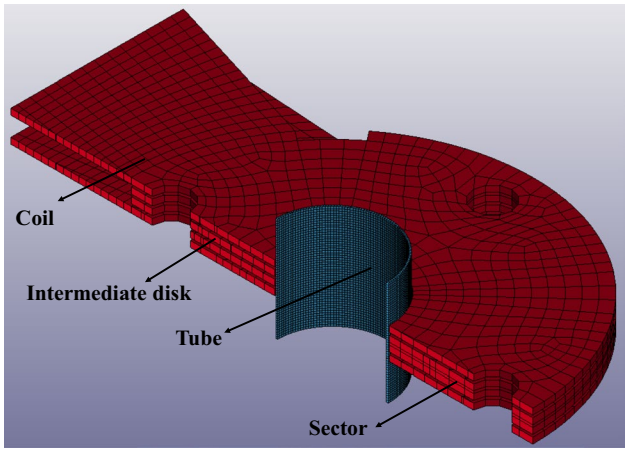

Fig. 4 The sectioned view of the FE model of coil and tube assembly

Table 7 Details of elements used in the FE model simulation for the coil and workpiece

Element type: hexahedral 3D elements			
Tube wall thickness (t) (mm)			Coil [OD/ID] (mm)
$t=1$	$t=1.7$	$t=2.4$	200/57
9152	19,188	19,552	4657

Lorentz force, and resultant velocity cannot be measured experimentally. However, they can be correlated with experimentally determined parameters such as rising time, peak current amplitude, and the degree of tube deformation, as presented in Table 8.

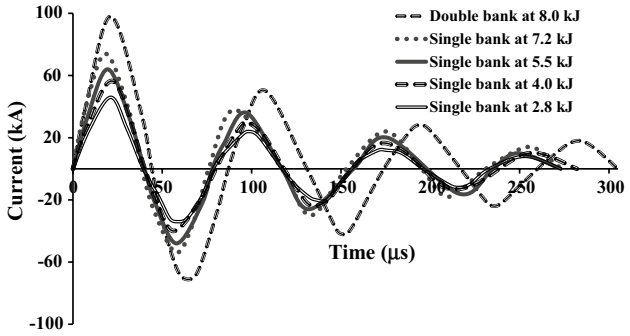

Fig. 5 The current pulses generated at different energy levels (banks) obtained through the Rogowski coil

The simulation results include peak values of the parameters, as presented in Table 8. The peak parameter values are obtained by interpreting the animated contour of the same for the entire duration in LS-PrePost software. These peak parameter values were correlated with the degree of tube deformation at different energy levels, the number of capacitor banks, and tube wall thickness. Figures 6 and 7 illustrate that a visual correlation between the numerical simulation and experiment results can be obtained by comparing the fringe of strain and photographs of the experimentally deformed tubes at different combinations of tube wall thicknesses, energy level, and the number of capacitor banks. A series of pictures illustrate numerical contours and experimentally deformed samples at different energy levels and tube wall thicknesses. The appearance of wrinkles, crest bottom, and ridges in both FE-simulated and experimentally deformed samples exhibited excellent similarity in patterns, and are nearly identical. An increase in the number of capacitor banks and energy levels resulted in a higher degree of deformation leading to more severe wrinkles. The increase in the thickness of the tube wall decreased the degree of tube deformation as evident from the fewer number of wrinkles. The wrinkles are more prominent in the tubes with lower thickness, namely 1 and 1.7 mm, for a similar level of applied energy. Thus, wrinkles are dependent on the applied energy level and tube thickness.

3.1 Effect of system parameters on deformation

There is an effect of the capacitance of the system on the current pulse system. It is inversely proportional to frequency. Thus, when the number of capacitors is increased, the capacitance of the system increases, and it can store higher energy. Figures 6 and 7 illustrate the degree of the tube deformation as the number of capacitor banks increased from one to two. The increase in the number of the capacitor banks increased the energy storage capacity from 4.0 to 8.0 kJ. A 56 mm OD tube compressed to 51.23 mm and 29.13 mm using a single and double bank, respectively. The 2.4 mm wall thickness tube at 4.0 kJ energy remained almost undeformed as compared to the one at 8.0 kJ energy. The

Table 8 Details of experimental parameters and resulting deformation of the workpiece

Tube dimension (OD-ID) (mm)	Thickness (mm)	Voltage (kV)/ energy (kJ)	No. of capacitor Bank	Rise time (µs)	Peak current (kA)	Final OD		
						Experimental (mm)	Simulation (mm)	% Age difference in OD
Single capacitor bank (04 capacitors of 14 µF)								
(56–54)	1.0 (w_1)	10/2.8	One	20	44	53.32	54.12	1.48
(56–54)	1.0 (w_1)	12/4.0	One	20	52	51.23	51.82	1.14
(56–54)	1.0 (w_1)	14/5.5	One	20	60	47.76	48.42	1.36
(56–54)	1.0 (w_1)	16/7.2	One	20	72	43.9	44.20	0.68
(56–52.6)	1.7 (w_2)	10/2.8	One	20	44	55.33	55.52	0.34
(56–52.6)	1.7 (w_2)	12/4.0	One	20	52	54.34	54.68	0.62
(56–52.6)	1.7 (w_2)	14/5.5	One	20	60	52.56	53.65	2.03
(56–52.6)	1.7 (w_2)	16/7.2	One	20	72	50.64	52.41	3.38
(56–51.2)	2.4 (w_3)	10/2.8	One	20	44	55.88	56.03	0.27
(56–51.2)	2.4 (w_3)	12/4.0	One	20	52	55.50	55.76	0.47
(56–51.2)	2.4 (w_3)	14/5.5	One	20	60	54.75	55.28	0.96
(56–51.2)	2.4 (w_3)	16/7.2	One	20	72	53.90	54.74	1.53
Double capacitor bank (08 capacitors of 14 µF)								
(56–54)	1.0 (w_1)	12/8.0	Two	22	94	29.13	27.26	6.86
(56–52.6)	1.7 (w_2)	12/8.0	Two	22	94	42.72	46.24	7.61
(56–51.2)	2.4 (w_3)	12/8.0	Two	22	94	49.44	51.29	3.61

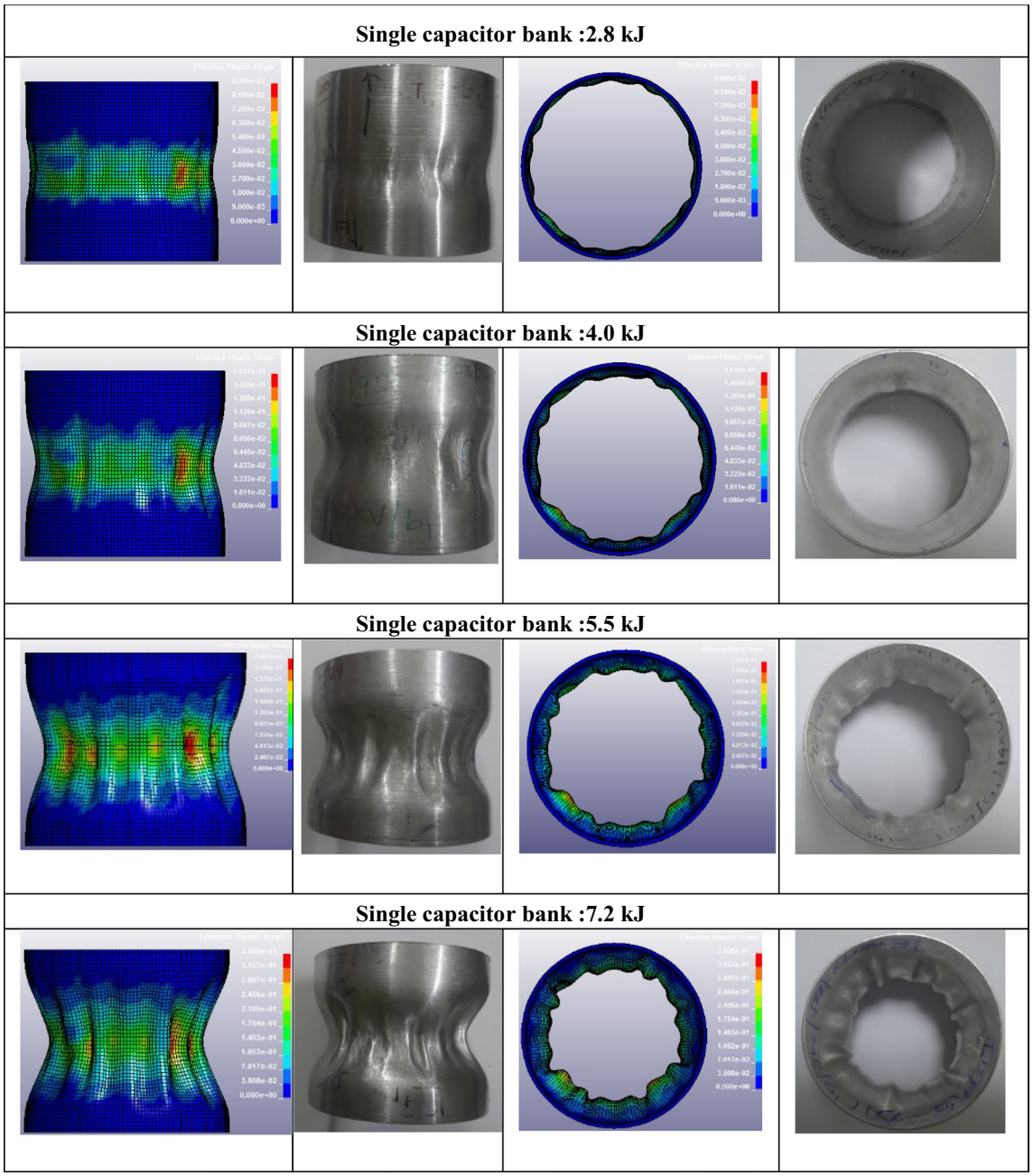

(a) Tube wall thickness (t)=1.0 mm

Fig. 6 The experimental vis-à-vis FE-simulated results showing the nature of deformation of the workpiece (tube) employing a single capacitor bank for different thicknesses and energy levels

numerically computed variation in other parameters such as resultant displacement, velocity, Lorentz force, and magnetic field is illustrated in Fig. 8. The parameter values exhibited a very significant increase when the number of the banks was increased.

Figure 8a illustrates the variation in displacement with the tube wall thickness and the single and double capacitor banks charged to the same level of voltage, namely 12 kV. A significant drop in the degree of deformation was observed as the tube wall thickness increased irrespective of the number of capacitor banks. The percentage decrease in deformation with an increase in the tube wall thickness was higher for a single capacitor bank than for a double capacitor bank assembly. The level of deformation (displacement) achieved by the 1 mm-thick tube with a single capacitor bank was identical to that by the 2.4 mm-thick tube with a double

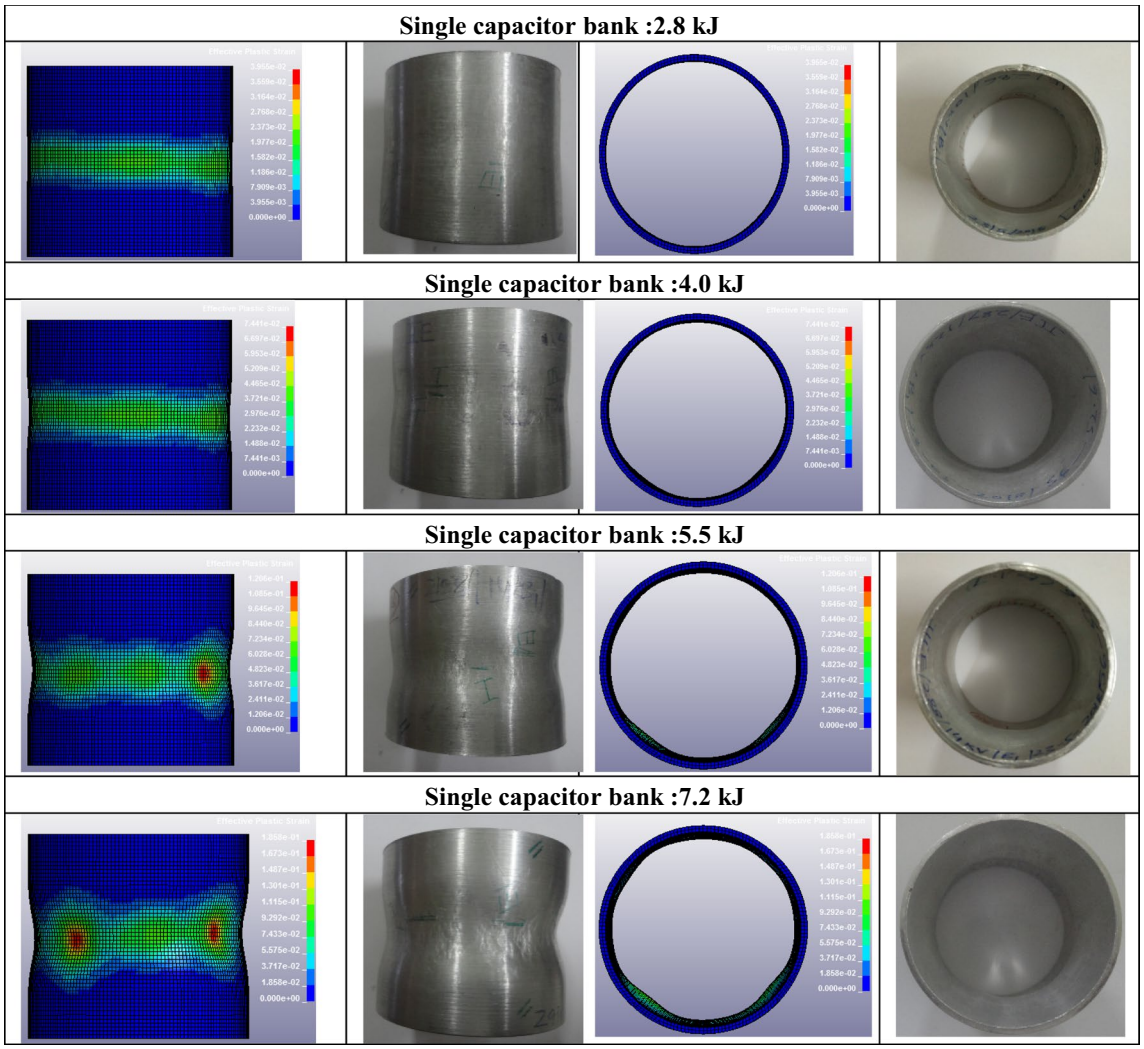

(b) Tube wall thickness (t)=1.7 mm

Fig. 6 (continued)

capacitor bank. The variation in peak velocity with the number of capacitor banks and tube wall thickness is illustrated in Fig. 8b. At the same charging voltage level, a three-to-fivefold increase in velocity was observed for the tube wall thickness in the range of 1–2.4 mm as the number of banks increased from single to double. The variation in the Lorentz force and magnetic field with the number of capacitor banks and tube wall thickness is shown in Figs. 8c, d, respectively. Both the parameters increased with an increase in the tube wall thickness from 1 to 1.7 mm and decreased thereafter with a further increase in thickness to 2.4 mm from 1.7 mm. Thus, for a given capacitor bank and coil, the maximum Lorentz force and magnetic field were achieved for the 1.7 mm-thick tube for both single and double capacitor banks probably due to skin depth, which was approximately 0.75 mm for both single and double capacitor banks. At this skin depth, the force causing deformation, namely Lorentz force, was more effective up to a tube wall thickness of 1.7 mm, since such a force develops as a body force unlike surface force in a conventional punch-blank arrangement. The body force acts across the thickness inside the body, whereas the surface force becomes effective on the surface only. Therefore, for higher wall thicknesses, the body force largely acts as a surface force beyond skin depth. The effects of the tube wall thickness on the Lorentz force and magnetic field showed the same trend for both single and double capacitor bank assemblies.

The hardness across the deformed samples was measured using the Vickers hardness machine at a 200 g force with 10 s dwell time to assess the deformation zone along the tube length. A sample that was deformed with 5.5 kJ energy using a single capacitor bank was cut in the middle and top upper zones and mounted on an epoxy base to measure hardness, as depicted in Fig. 9. Hardness was higher in the middle

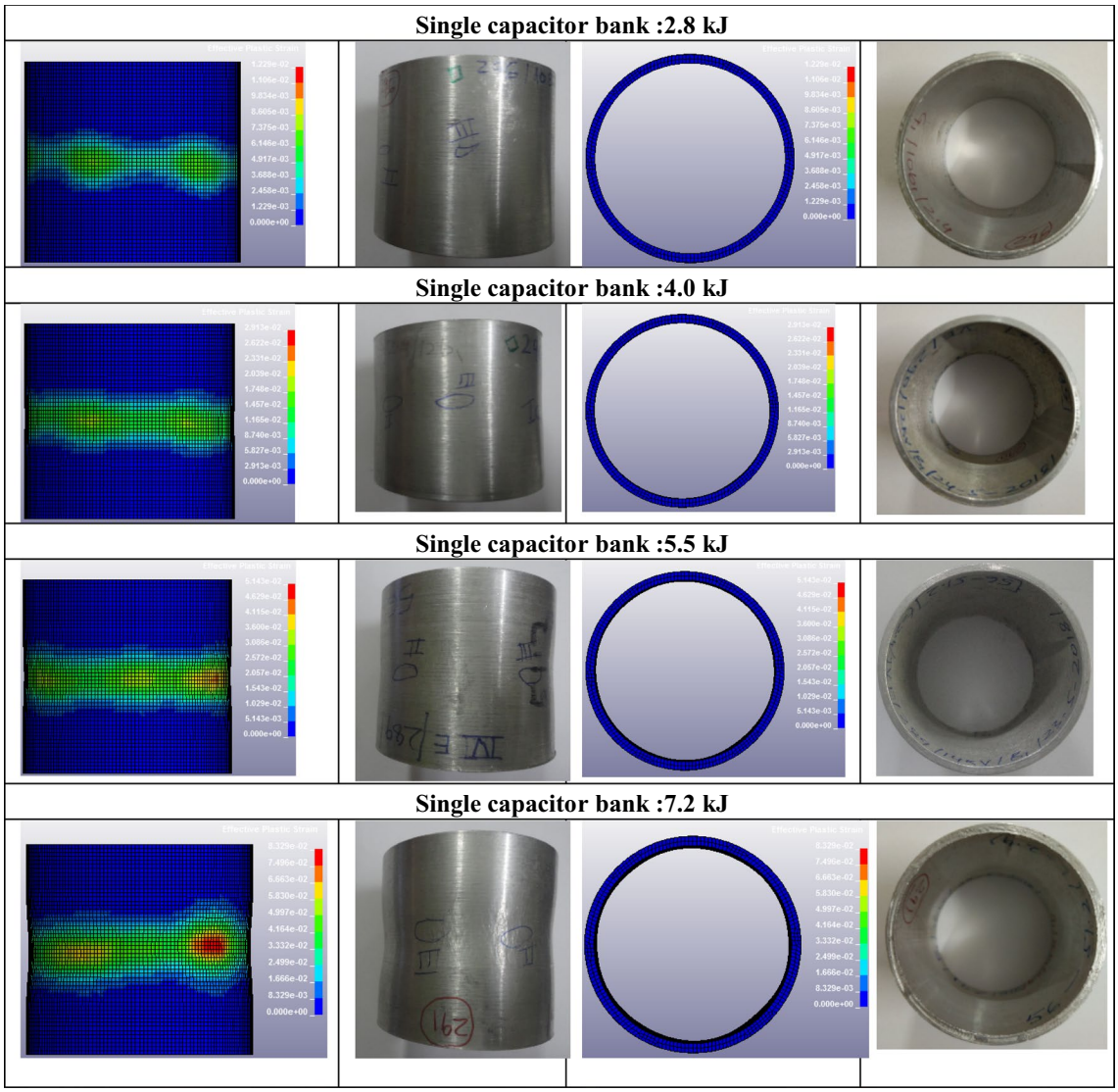

(c) Tube wall thickness (t)=2.4 mm

Fig. 6 (continued)

(63.25 HV) than on the upper side (51.76 HV), thereby confirming that the sample was deformed more severely in the middle than in the upper or bottom regions. Skin depth (δ) is the factor that estimates the thickness of the layer across the total tube thickness to within, which induced current to be distributed on the surface of the tube. It depends on the frequency of the pulse as follows:

$$\delta = \sqrt{\frac{\rho}{\pi f \mu_0}}, \tag{1}$$

where ρ is the electrical resistivity of the workpiece (ohm-meter), f is the frequency of the current (Hertz), and μ_0 is the permeability of free space (H/m).

The equation shows that the current discharged from a single capacitor bank at 12.6-kHz frequency produced 0.747 mm of skin depth. Similarly, a double capacitor bank operated at 11.4-kHz frequency produced 0.785 mm of skin depth. Thus, all the samples utilized and dissipated the applied energy entirely because the thickness of the workpiece was higher than 1 mm.

The frequency and its rise time at different energy levels for the single and double capacitor banks are illustrated in Fig. 10. Energy had no effect on the frequency and rise time for the same capacitor bank even when charged to different voltage levels. Moreover, the increase in voltage increased the peak value of the current pulse for the same capacitor bank. However, when the number of capacitor banks

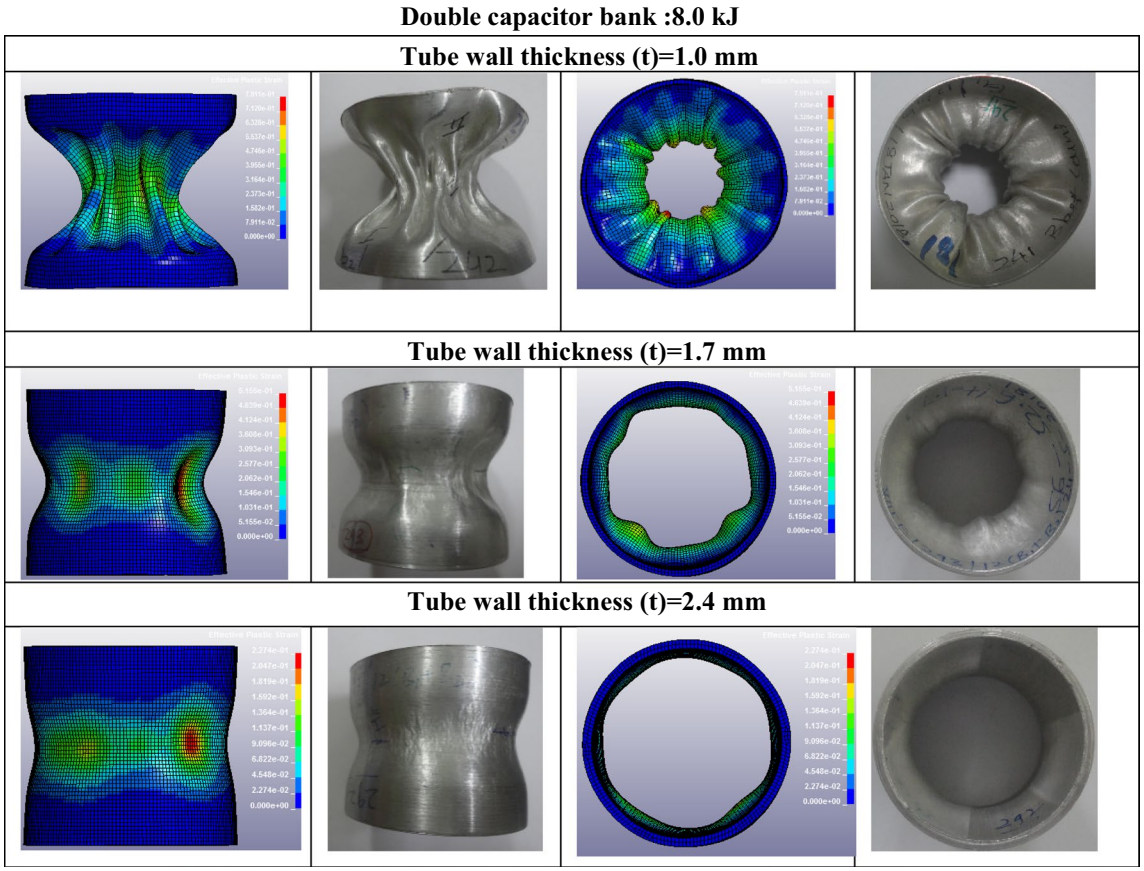

Fig. 7 A comparison of the nature/extent of deformation of the workpiece experimentally with the FE-simulated ones employing a double capacitor bank for different thicknesses (*t*) of the workpiece (Al tube) at the energy level of 8 kJ

increased from single to double, the frequency decreased and rise time increased because of its dependence on the inductance of the system. Moreover, the current intensity increased with the increasing energy level.

3.2 Variation in displacement and velocity with energy and wall thickness of the workpiece

The increase in tube wall thickness demonstrated a decrease in the tube deformation level (Fig. 11a), whereas for the same wall thickness of the tube, the resultant displacement increased with increasing energy levels. However, the extent of increase was more for the 1-mm-thick tube than for the tubes with wall thicknesses of 1.7 and 2.4 mm. The 2.4-mm-thick tube did not show any significant deformation with the increase in energy levels from 2.8 to 7.2 kJ with a single capacitor bank. On the contrary, the deformation nearly tripled with 2 capacitor banks at approximately 1-kJ higher energy. At the same level of energy, the degree of deformation decreased to a greater extent when the wall thickness increased from 1 to 1.7 mm compared with that when the thickness increased from 1.7 to 2.4 mm, proving that the tube with higher thickness was less sensitive to deformation compared with the tube with lower thickness (Fig. 11a). To analyze further, a tube of 1-mm wall thickness can be deformed by 18 mm with a double capacitor bank compared with just 11.4 mm with a single bank at the same level of charging. Figure 11b depicts the velocity of tube deformation as a function of the wall thickness of the tube at different energy levels. The velocity depicted a similar variation trend for all energy levels. Very high velocity could be achieved when the number of capacitor banks increased from 1 to 2. A tube of 1-mm wall thickness attained a higher deformation velocity of 497 m/s with a double capacitor bank at 8.0 kJ energy than with a single capacitor bank at 7.2 kJ of energy; the deformation velocity with a single capacitor bank was 384 m/s.

3.3 Variation in current density, magnetic field, and Lorentz force with energy and thickness of the workpiece

The current density, magnetic field, and Lorentz force are interrelated parameters, and they depend on the skin depth.

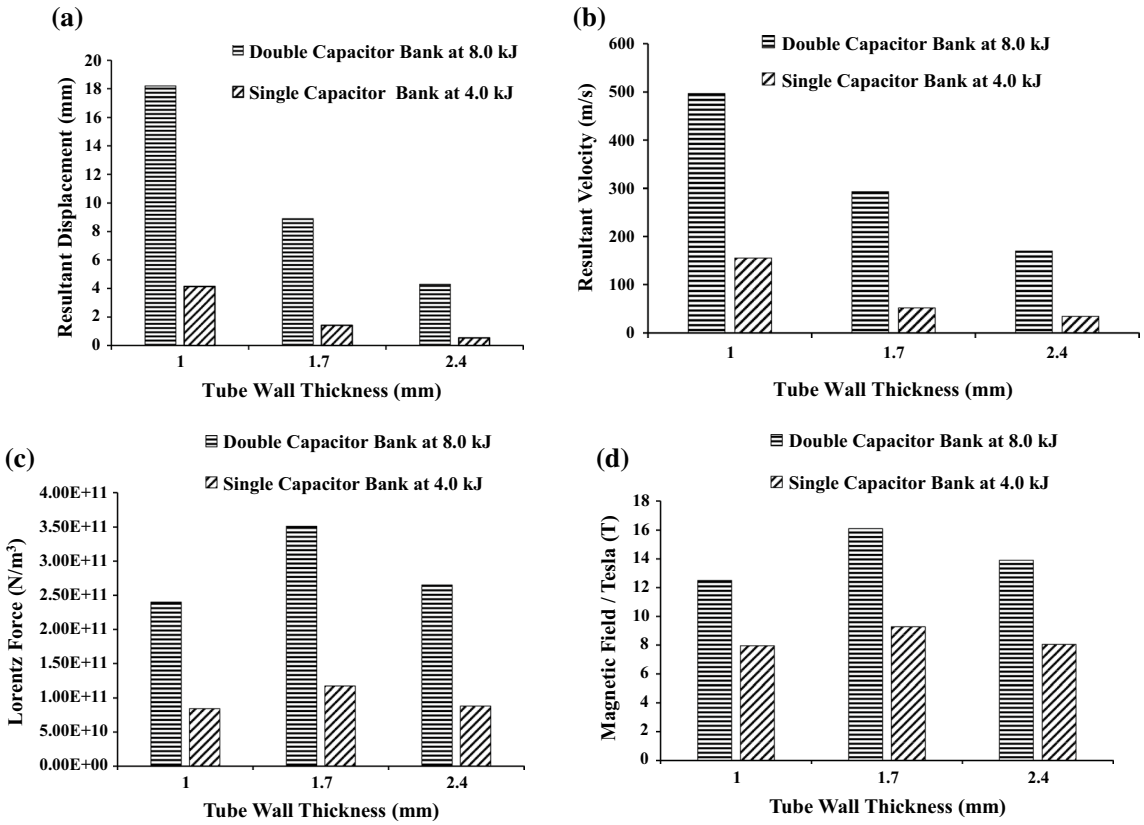

Fig. 8 The effect on parameters at single and double capacitor banks

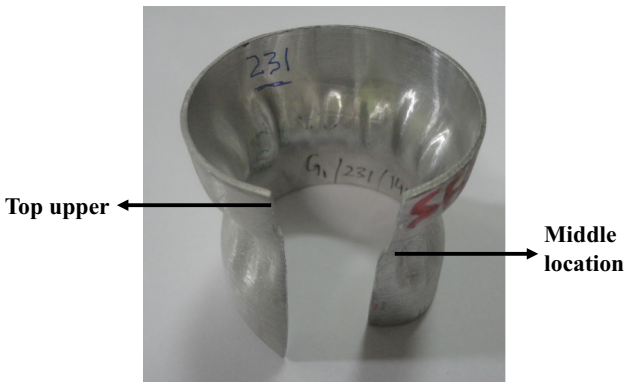

Fig. 9 The sample showing the location for hardness

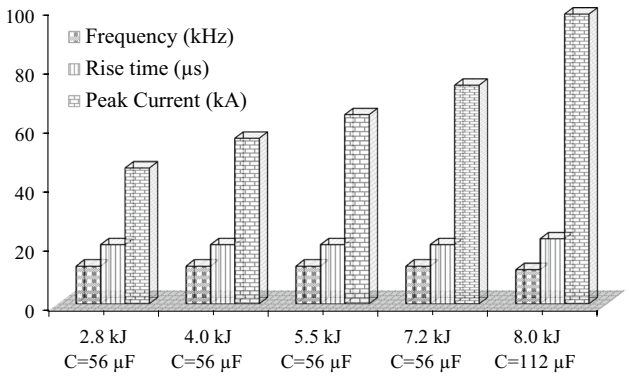

Fig. 10 The variation in current frequency, rise time, and peak current attained with a single and double capacitor banks

These parameters increased when the tube wall thickness increased from 1 to 1.7 mm, but decreased with a further increase in the tube wall thickness to 2.4 mm (Figs. 12, 13). The concept of body force, as discussed in the previous section, can be attributed to this trend. Thus, the tube thickness can be made approximately double to harness the maximum efficiency of deformation. This trend was similar for both single and double banks.

4 Conclusions

AA6061 tubes of different wall thicknesses were deformed electromagnetically at different energy levels to analyze their deformation behavior as a function of the applied energy level and thickness of the workpiece. FE simulation was also performed to correlate the nature and degree of

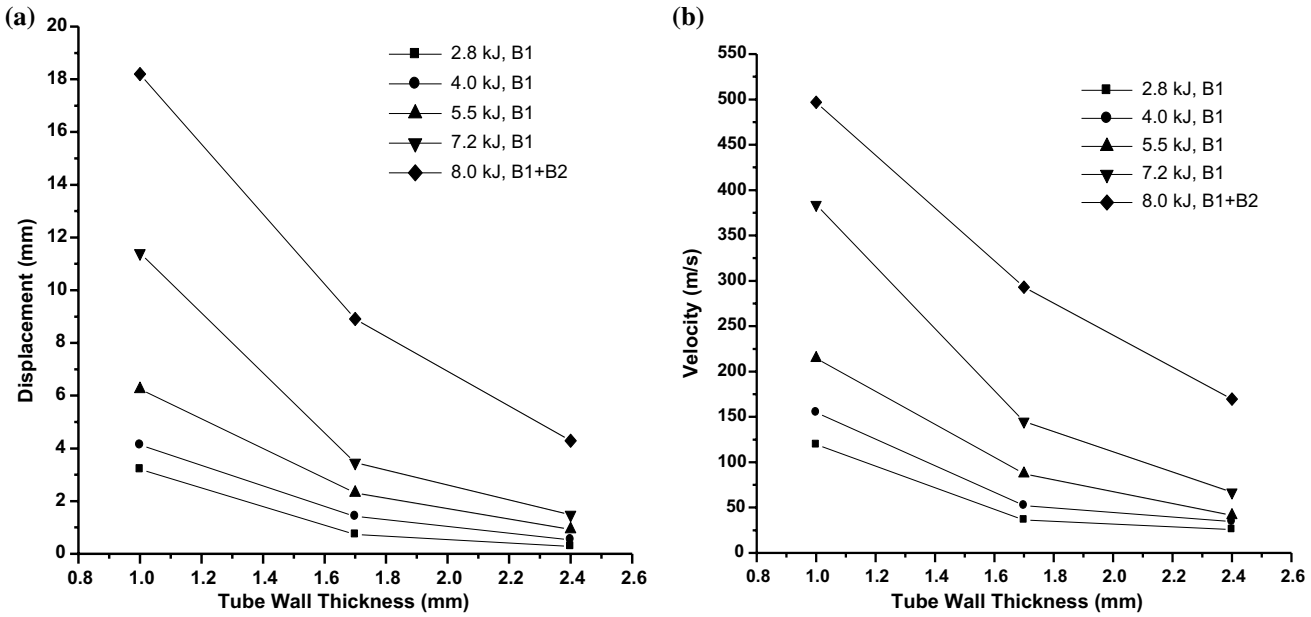

Fig. 11 The degree of deformation (displacement) and velocity as a function of tube wall thickness

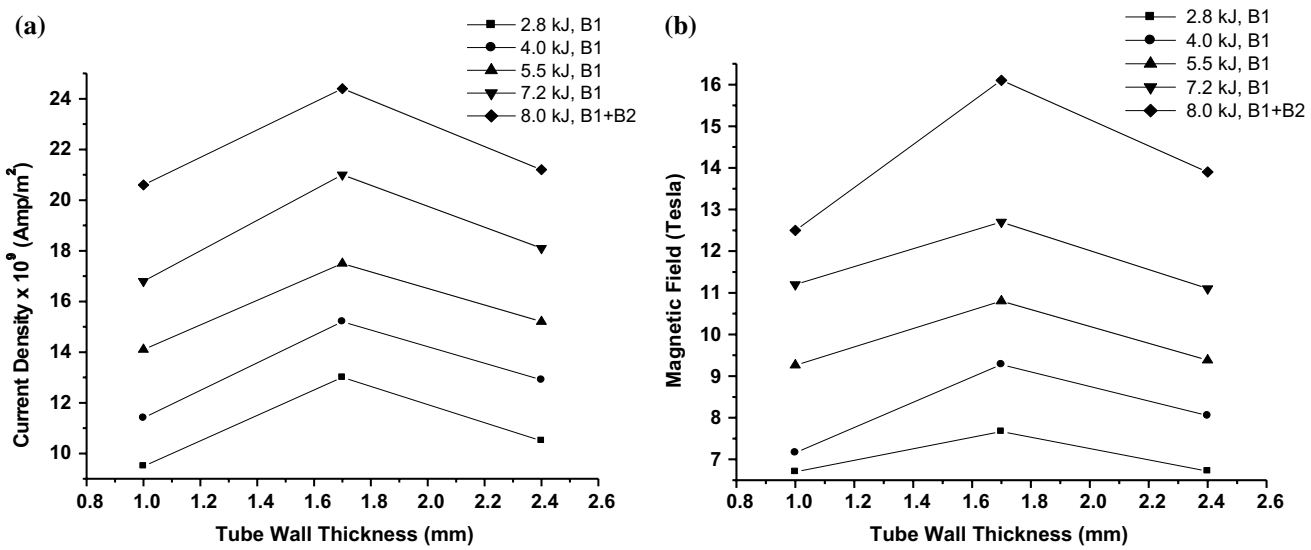

Fig. 12 The current density and magnetic field as a function of wall thickness and energy level

deformation with process parameters. Experiments were conducted at different energy levels (2.8, 4.0, 5.5, 7.2, and 8.0 kJ) and using capacitor banks (single and double) at a 0.5 mm constant gap between the coil and tube. The results are summarized as follows:

1. Numerical simulation of tube deformation was performed as per the experimental matrix to correlate tube deformation at different energy levels and tube thicknesses. The results showed a reasonably good agreement with the experimental results, with an acceptable range of variation (0.27–7.61%).
2. The number of capacitor banks had a significant effect on the nature and extent of tube deformation. When the number of capacitor banks increased, the frequency decreased and energy increased, leading to a higher degree of deformation. The number of wrinkles was higher for thinner tubes at the same applied energy level. Furthermore, higher tube thickness presented with no wrinkles even at higher energy levels with 2 capacitor

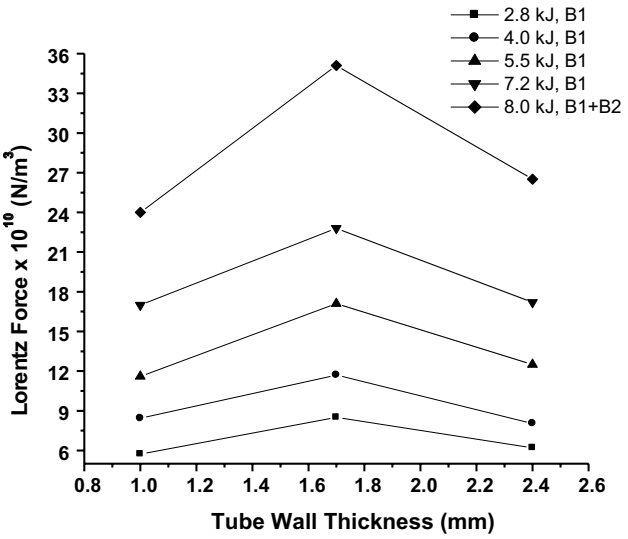

Fig. 13 The Lorentz force as a function of tube wall thickness and energy level

banks. Thus, there is a limit to the thickness and energy level to be applied to achieve deformation without wrinkles.

3. The degree of deformation (displacement) decreased with an increase in the tube wall thickness. The tube with 1 mm wall thickness experienced the maximum degree of displacement at the highest velocity. Moreover, the degree of tube deformation was more in the case of the double capacitor bank than the single capacitor bank.
4. The Lorentz force, magnetic field, and current density increased with an increase in the tube wall thickness up to a thickness of 1.7 mm. However, the values of these parameters decreased with a further increase in the tube wall thickness. Thus, an optimum tube wall thickness should be maintained to achieve an optimum Lorentz force, magnetic field, and current density.

Acknowledgements The authors thank the Director, CSIR-AMPRI, Bhopal; Mr. Rakesh Kaul, Head, LMPD, RRCAT, Indore; and Dr. P. Ganesh, Scientific officer (G), RRCAT, Indore for providing facilities for carrying out the study.

References

1. Yu HP, Li CF (2007) Effects of coil length on tube compression in electromagnetic forming. Trans Nonferr Met Soc China 17(6):1270–1275
2. Bartels G, Schätzing W, Scheibe HP, Leone M (2009) Comparison of two different simulation algorithms for the electromagnetic tube compression. Int J Mater Form 2(1):693
3. Shabanpour M, Arezoodar AF (2016) Multi-objective optimization of the depth of bead and tearing in electromagnetic tube compression forming. Int J Adv Manuf Technol 87(1–4):867–875
4. Haratmeh HE, Arezoodar AF, Farzin M (2017) Numerical and experimental investigation of inward tube electromagnetic forming. Int J Adv Manuf Technol 88(5–8):1175–1185
5. Savadkoohian H, Arezoodar AF, Arezoo B (2017) Analytical and experimental study of wrinkling in electromagnetic tube compression. Int J Adv Manuf Technol 93(1–4):901–914
6. Demir OK, Psyk V, Tekkaya AE (2010) Simulation of tube wrinkling in electromagnetic compression. Prod Eng Res Dev 4(4):421–426
7. Guo YB, Wen Q, Horstemeyer MF (2005) An internal state variable plasticity-based approach to determine dynamic loading history effects on the material property in manufacturing processes. Int J Mech Sci 47(9):1423–1441
8. Gharghabi P, Dordizadeh P, Niayesh K (2011) Impact of metal thickness and field shaper on the time-varying processes during impulse electromagnetic forming in tubular geometries. J Korean Phys Soc 59(61):3560–3566
9. Zhong L, Lu C, Shujie L, Mei W, Junping L (2015) Electromagnetic forming with solenoid coil. In: Seventh international conference on measuring technology and mechatronics automation, IEEE, 13–14 June 2015, Nanchang, China
10. Park H, Lee J, Kim SJ, Lee Y, Kim D (2016) Parametric study on numerical simulation of the electromagnetic forming of DP780 steel workpiece with aluminum driver sheet. J Phys Conf Ser 734(3):032085
11. Cui X, Mo J, Li J, Xiao X (2017) Tube bulging process using multidirectional magnetic pressure. Int J Adv Manuf Technol 90(5–8):2075–2082
12. Haiping YU, Chunfeng LI (2009) Effects of current frequency on electromagnetic tube compression. J Mater Proc Technol 209(2):1053–1059
13. Ahmed M, Panthi SK, Ramakrishnan N, Jha AK, Yegneswaran AH, Dasgupta R, Ahmed S (2011) Alternative flat coil design for electromagnetic forming using FEM. Trans Nonferr Met Soc China 21(3):618–625
14. Vivek A, Kim KH, Daehn GS (2011) Simulation and instrumentation of electromagnetic compression of steel tubes. J Mater Proc Technol 211(5):840–850
15. Shang J, Hatkevich S, Wilkerson L (2012) Comparison between experimental and numerical results of electromagnetic tube expansion. In: 12th international LS-DYNA users conference, 3–5 June 2012, Detroit, USA
16. Cao Q, Han X, Lai Z, Xiong Q, Zhang X, Chen Q, Xiao H, Li L (2015) Analysis and reduction of coil temperature rise in electromagnetic forming. J Mater Proc Technol 225:185–194
17. Rajak AK, Kore SD (2018) Numerical simulation and experimental study on electromagnetic crimping of the aluminium terminal to copper wire strands. Electr Power Syst Res 163:744–753
18. Li C, Zhao Z, Li J, Li Z (2005) The effect of tube length on magnetic pressure in tube electromagnetic bulging. J Mater Proc Technol 166(3):381–386
19. Johnson GR, Cook WH (1985) Fracture characteristics of three metals subjected to various strains, strain rates, temperatures, and pressures. Eng Fract Mech 21(1):31–48
20. Psyk V, Risch D, Kinsey BL, Tekkaya AE, Kleiner M (2011) Electromagnetic forming—a review. J Mater Proc Technol 211(5):787–829
21. Doley JK, Kore SD (2016) A study on friction stir welding of dissimilar thin sheets of aluminum alloys AA5052–AA6061. J Manuf Sci Eng 138(11):114502

22. Zhang X, Zhang M, Sun L, Li C (2018) Numerical simulation and experimental investigations on TA1 titanium alloy rivet in electromagnetic riveting. Arch Civ Mech Eng 18(3):887–901
23. Wang Z, Chen C, Liu C, Gao T (2019) Research on electromagnetic tube compression of small diameter aluminum alloy tube and efficiency of field shaper. J Braz Soc Mech Sci Eng 41(4):177